Seasonal, weathering and water use controls of silicon cycling along the river flow in two contrasting basins of South India

P.K. Sarath, K.R. Mangalaa, Damien Cardinal, G.P. Gurumurthy, Arnaud Dapoigny, V.V.S.S. Sarma, J. Riotte

Chemical Geology 604 (2022) 120883

Contents lists available at ScienceDirect

Chemical Geology

journal homepage: www.elsevier.com/locate/chemgeo

Seasonal, weathering and water use controls of silicon cycling along the river flow in two contrasting basins of South India

P.K. Sarath [a,*], K.R. Mangalaa [a,1], D. Cardinal [a], G.P. Gurumurthy [d], A. Dapoigny [e], V.V.S.S. Sarma [f], J. Riotte [b,c]

[a] LOCEAN-IPSL, Sorbonne Université (SU, CNRS, IRD MNHN), Paris 75005, France
[b] Géosciences Environnement Toulouse - GET (IRD, CNRS, CNES, Université Toulouse III), 31400 Toulouse, France
[c] Indo-French Cell for Water Sciences, IRD, Indian Institute of Science, Bangalore, 560012, India
[d] Birbal Sahni Institute of Palaeosciences (BSIP), Lucknow 226007, Uttar Pradesh, India
[e] LSCE-IPSL, CEA-CNRS-UVSQ, Universite Paris Saclay, 91198 Gif-sur-Yvette, France
[f] National Institute of Oceanography–CSIR (NIO), Regional Centre of Visakhapatnam, 530017, India

ARTICLE INFO

Editor: Dr Oleg Pokrovsky

Keywords:
Silicon isotopes
Tropical rivers
Dissolved silicon
Kaveri
Netravathi

ABSTRACT

We present the first study of river water silicon isotopic composition from two contrasting basins in South India, the east flowing Kaveri river and the west flowing Netravathi river. Both rivers originate from the Western Ghats. River water samples were collected from mainstream, tributaries and reservoirs at different locations along the river flow during dry and wet (monsoon) seasons, with an additional post-monsoon sampling in Netravathi. High rainfall in Netravathi basin and upper reaches of Kaveri induce intense weathering in the region, with superposing contribution from anthropogenic controls in downstream Kaveri. The $\delta^{30}Si_{DSi}$ values range from +0.42 to +1.65‰ for Netravathi river basin and + 0.32 to +2.85‰ for Kaveri river basin. Silicate weathering index (R_e) shows intense weathering associated with monosiallitization (kaolinite-gibbsite formation) in Netravathi basin and relatively moderate weathering with bisiallitization (smectite-kaolinite formation) in Kaveri basin. The seasonal changes in $\delta^{30}Si_{DSi}$ and R_e in each basin shows similar patterns, with a likely higher and heavier contribution of soil water from deeper soil profiles closer to weathering front and bedrock, associated with significant secondary mineral formation during dry season and leaching of superficial soil profiles during the high discharge periods of monsoon. We provide a theoretical framework to estimate relative contribution of silicate weathering vs. anthropogenic processes on riverine $\delta^{30}Si_{DSi.}$ R_e is broadly correlated with $\delta^{30}Si_{DSi}$ and an isotopic mass balance involving the whole rock composition (excluding the stable quartz and sericite) shows that the $\delta^{30}Si$ in river water are well explained by silicate weathering and gibbsite-kaolinite formation in the Netravathi and upper upper reaches of Kaveri. However, silicate weathering explains only partially the heavier $\delta^{30}Si_{DSi}$ signatures in the middle and lower reaches of the Kaveri, and the additional enrichment of about +1.06‰ can be attributed to uptake of silicon and Si-depleted return flow through irrigated agriculture in the basin. This study confirms the major control of pedoclimatic conditions on the $\delta^{30}Si$ of rivers and provides for the first time an estimation of the impact of human activities on the silicon isotopic signature of rivers.

1. Introduction

Silicon (Si) is the second most abundant element in the Earth's crust and is present in particulate and dissolved forms in rivers, estuaries and oceans. Chemical weathering is the major source of Si supply to the terrestrial and aquatic systems. During chemical weathering of primary silicate minerals, silicon is partly released as a solute (dissolved silicon, DSi hereafter), with an intermediate behaviour in between the one of typical soluble elements with low ionic radius to charge ratio (r/z) that form oxyanions (similar to elements such as S, P, N, C), while the other Si fraction is immobilized into secondary clay minerals (similar to poorly soluble element with medium r/z e.g. Al). Silicon has three stable isotopes, ^{28}Si (92.2%), ^{29}Si (4.7%) and ^{30}Si (3.1%) with their respective percentage of terrestrial abundance (Poitrasson, 2017). The formation of

* Corresponding author.
E-mail address: sarath.pullyottum-kavil@locean.ipsl.fr (P.K. Sarath).
[1] Now at: Ministry of Earth Sciences, Prithvi Bhawan, Lodhi road, New Delhi, 110003, India.

https://doi.org/10.1016/j.chemgeo.2022.120883
Received 20 October 2021; Received in revised form 11 April 2022; Accepted 22 April 2022
Available online 27 April 2022

secondary minerals during silicate weathering can lead to preferential incorporation of lighter Si isotope which leads to enrichment of isotopically heavy DSi with a higher δ^{30}Si value (up to +4.7‰) compared to unweathered silicate rocks (−0.3‰; Savage et al., 2013, Savage et al., 2012; Poitrasson, 2017). DSi is largely dominated by orthosilicic acid, H_4SiO_4 (>98% at pH <8) and serves as an important nutrient for aquatic silicifying organisms and, terrestrial plants defense against biotic and abiotic stress. Indeed, vegetation plays an important role in Si biogeochemical cycle via precipitation of phytoliths (amorphous or biogenic silica, BSi) that are recycled into the soil or exported to rivers through erosion (Alexandre et al., 1997; Derry et al., 2005). In aquatic systems, diatom uptake also alters the Si biogeochemical cycle via conversion of DSi to biogenic silica (BSi) (Conley, 1997). Si uptake and biomineralization by biological process also leads to preferential incorporation of ^{28}Si enriching the DSi pool in heavy isotopes. Consequently, these continental processes control the Si supply to the estuaries and coastal waters which represents 70% of external DSi supply to the ocean (Tréguer et al., 2021). Urbanization and anthropogenic activities like agriculture and construction of reservoirs can reduce the supply of Si to estuarine and coastal ecosystems. Such effects are well documented in several aquatic environments (Conley et al., 2000; Humborg et al., 2002; Hughes et al., 2012; Meunier et al., 2015). Deforestation can enhance the soil erosion leading to increase in DSi supply into aquatic ecosystems (Struyf et al., 2010; Vandevenne et al., 2012; Mangalaa et al., 2017). Increasing anthropogenic activities have drawn much attention to understand their impact on the global biogeochemical Si cycle. Tropical rivers are known for their high DSi flux because of warm and wet climatic conditions, which favour intense chemical and physical weathering and runoff (Hughes et al., 2012; Dürr et al., 2011). Hence, the understanding of the Si cycle in tropical regions is of particularly high relevance in this context. In recent years, Si isotopes have been proved to be a valuable tool for tracing several processes affecting the Si biogeochemical cycle such as secondary mineral formation (Georg et al., 2007), mixing of the different DSi sources (Georg et al., 2006a, 2006b), biological uptake (Ding et al., 2004; Engström et al., 2010), anthropogenic effects such as damming (Hughes et al., 2012) and land use (Delvaux et al., 2013).

Despite being the major contributor of DSi to the ocean, many tropical rivers remain understudied. This results in large uncertainties in estimating net DSi fluxes to the ocean (±25%, Tréguer et al., 2021). In the present work, we study the Si cycle in two contrasting tropical rivers of Southern India, Kaveri (also known as Cauvery) and Netravathi. Both river headwaters originate from the Western Ghats, but the Kaveri basin is draining eastward to the Bay of Bengal while the Netravathi flows westward to the Arabian Sea. Because of the very humid climate along the western coast, the Netravathi basin experiences intense weathering and higher Si supply to the coast compared to Kaveri (Gurumurthy et al., 2012). The upper Kaveri basin is characterized by a sharp rainfall gradient, from 3000 mm/yr to about 500 mm/yr within a span of 100 km. Most of the Kaveri basin experiences semi-arid to sub-humid conditions (Meunier et al., 2015). Such contrasting land use and climate in these two tropical rivers make the comparison of both systems particularly interesting for understanding how Si cycle gets affected by natural (weathering) and anthropogenic (agricultural land use) pressures.

Therefore, we aim 1) to determine the seasonal variability of silicon isotopic signature in the Kaveri and Netravathi river basins and to identify the factors driving the Si isotopic compositions in these two river systems, and 2) to understand the effects of weathering, climate, and anthropogenic activities on the Si cycle along the river course before entering the estuaries.

2. Study area and methods

2.1. River Settings, climate and hydrology

Kaveri basin is located between 10° 07 'N to 13° 28' N and 75° 28′E to 79° 52′E. The river runs about 765 km towards the southeast and drains an area of 85,626 km^2 from the Western Ghats to the Bay of Bengal (Fig. 1a) and drains three states of India with 41% in Karnataka (source of Kaveri, Thala Kaveri), 55% in Tamil Nadu and the remaining 3% in Kerala. Kaveri river basin covers a major part of the South Indian peninsula and is constituted by three sub-basins namely upper (Western Ghats), middle (Mysore plateau) and lower (delta) basins. The important tributaries joining the Kaveri are Hemavathi (H), Kabini (K), Shimsha (S) and Arkavathi (A), Bhavani (Fig. 1a). The Kaveri river basin experiences tropical monsoon climate with influence of southwest (SW) monsoon (June to September) in upper basin and northeast (NE) monsoon in lower basin (October–November). The Western Ghats create a rain shadow that affects the SW monsoonal winds in the East inducing on the Deccan Plateau a sharp rainfall gradient from West (humid) to East (semi-arid). Therefore, Kaveri basin receives maximum rainfall during SW monsoon mainly in the upper reaches and partly in middle reaches which are responsible for 80% of the annual water flow and sediment load (Pattanaik et al., 2013). Hence, the spatial rainfall distribution ranges from 6000 mm/yr in the Western Ghats, to 300 mm/yr in the eastern parts during NE monsoon (Meunier et al., 2015). The catchments of Arkavathi and Shimsha tributaries, which receive only 700–800 mm/yr rainfall, i.e., semi-arid conditions, are exposed to diverse urban and agriculture pollutions. The Arkavathi river especially drains Bangalore and is considerably polluted (35 to 45% pollution index, based on anions potentially brought by human activities (SO_4^{2-}, NO_3^- and Cl^-) compared to alkalinity, Pacheco and van der Weijden, 1996). Both Arkavathi and Shimsha discharges are controlled by numerous dams, which are limiting the flow towards the Kaveri to a mixture of domestic and industrial effluents (Lele et al., 2013), return flow from irrigated agriculture (paddy fields) and local groundwater contribution. The historical runoff of the Kaveri used to be 21.3 km^3 yr^{-1} i.e., 262mm/yr (Integrated Hydrological Data Book, 2012, cited by Meunier et al., 2015) but diversion of water to meet domestic and irrigation demands accounts for 80% of total runoff, resulting in a low discharge of just 4.5 km^3 yr^{-1} to the sea (Meunier et al., 2015). Agriculture is the major land use in the Kaveri basin covering 66% of the total area, followed by forest cover (20%, WRIS. Kaveri Basin Report: Govt. of India, 2014).

The Netravathi basin – lies between 12°29′11″N to 13°11'11″N and 74° 49′08″E to 75°47′53″E and is surrounded by Tunga-Bhadra basin in the North, Kaveri basin in the East and by the Arabian Sea in the West. It originates from densely forested Western Ghats (Chikmagalore) and runs about 147 km southwest to the Arabian Sea forming a common estuary with Gurupur river at Mangalore (Fig. 1b). The total drainage area of the basin is 3657 km^2. The major tributaries of Netravathi basin are Shanthimageru (Sha), Gundiya hole (Gun), Shishilahole (Shi) and Neriya hole (Ner) (Fig. 1b). The basin is characterized by high humidity and heavy rainfall (3600–4200 mmyr^{-1}, data from http://www.imd.gov.in cited by Gurumurthy et al., 2012). Similar to upper Kaveri basin, the river flow is controlled by the SW monsoon with 94% of total discharge occurring during June to October (Gurumurthy et al., 2012, Gurumurthy et al., 2014). The annual discharge from the river Netravathi is 12 km^3 yr^{-1} (Karnataka Irrigation Department 1986 cited by Gurumurthy et al., 2012). Upper basin situated in the western ghats is densely forested, limiting erosion in the basin (Ganasri and Ramesh, 2016). The major contrasting features of both river basins are summarised in Table 1.

2.2. Geology of Kaveri and Netravathi Basin

2.2.1. Kaveri

The upper and middle reaches of the basin are composed of a silicate Precambrian basement comprising peninsular gneiss, charnockites and granitic rocks associated with metasedimentary and mafic rocks (Naqvi and Rogers, 1987; Shadakshara Swamy et al., 1995). The lower reaches of Shimsha drain mafic granulite, foliated charnockites and granitoid

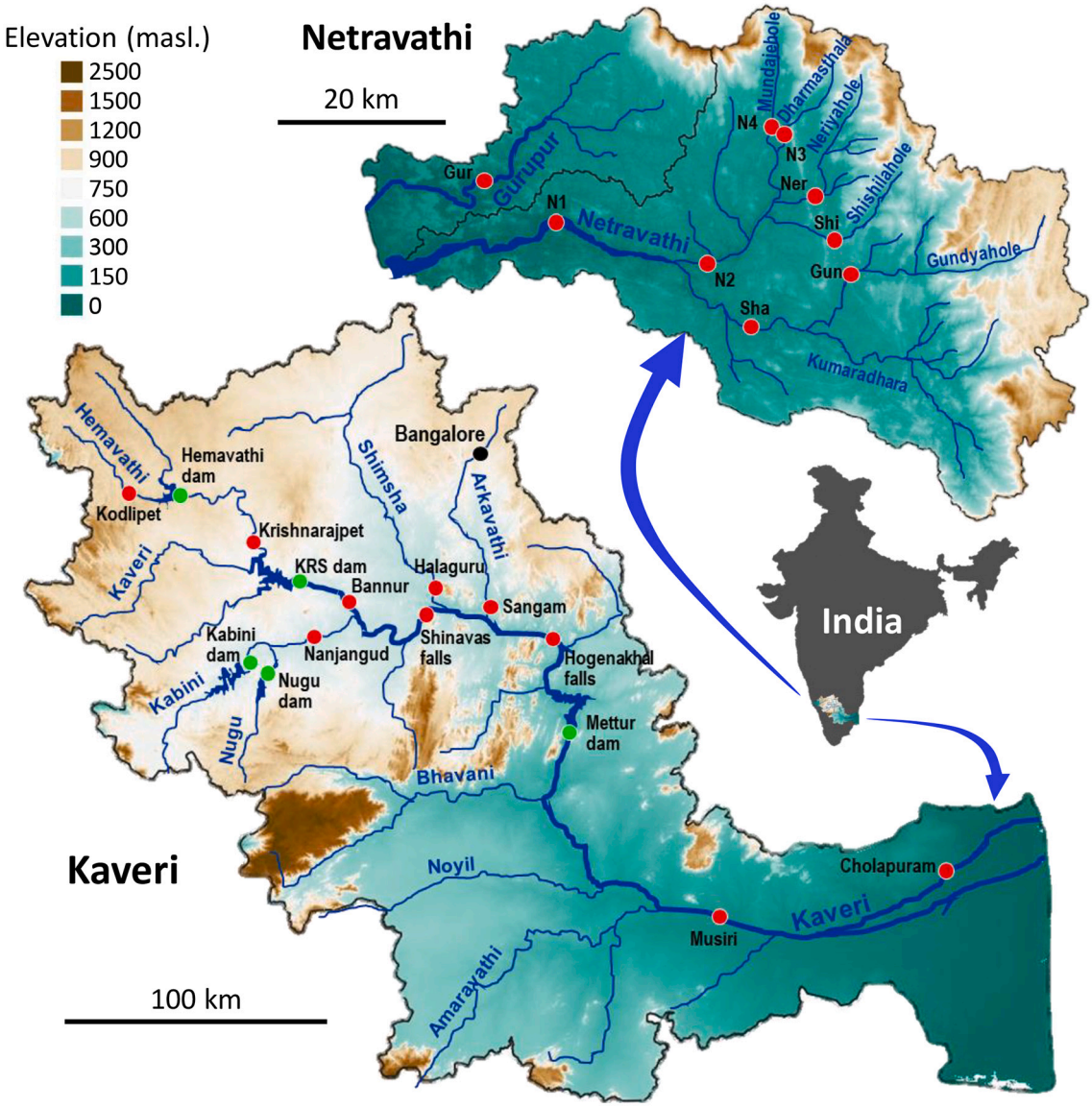

Fig. 1. Location maps of Kaveri/Cauvery (a) and Netravathi (b) basins showing the sampling stations (samples from dam/reservoir is indicated in green filled circles and river water in red circles), (b) Netravathi mainstream sampling stations are indicated by the letter "N" and the numbers are the station number. Tributaries of Netravathi basin are indicated by their first three letters (for example, Sha = Shanthimugeru, Gun = Gundyahole etc.). "Gur" represents Gurupur river, flowing adjacent to the Netravathi basin (modified from Meunier et al., 2015 and Gurumurthy et al., 2012).

gneisses (Pattanaik et al., 2013). The lower reaches of Kaveri flow through the Cretaceous deposits composed of conglomeratic sandstone, limestone, shale and finally the alluvium plains (Pattanaik et al., 2007). The $\delta^{30}Si$ of the gneiss bedrock from Mule Hole in Kaveri basin reported by Riotte et al. (2018) is at -0.34 ± 0.08‰. The Precambrian gneiss is a part of TTG (Tonalite–trondhjemite–granodiorite) felsic source rocks but it is a metasediment, which is probably why it is quite light compared to some other Archean rocks (André et al., 2019). The weathered layer (regolith) consists of thick laterite in the humid zone, ferralsol/vertisol developed on saprolite in semi-arid zone of upper and middle reaches, and alluvium in the lower reaches.

2.2.2. Netravathi

The basin primarily drains the metamorphic changeover zone of west dharwar craton comprising trondhjemite – tonalite - granodiorite suite (Naqvi and Rogers, 1987). Overall, the basin is composed of 83% migmatites and granodiorites, 6% metasediments, 5% charnockites and 2% amphibolites (Gurumurthy et al., 2012, 2015a, 2015b) (Fig. 1b). The regolith thickness ranges from 20 to 30 m and is primarily composed of thick laterites (Gurumurthy et al., 2012).

2.3. Materials and methods

2.3.1. Sampling and determination of major elements concentrations

In Kaveri basin, the water samples were collected in 10 riverine and 5 dam stations during dry season (May 2007) and southwest monsoon/wet season (July 2007). In Netravathi basin, the samples were collected at 9 riverine stations (no reservoirs) during dry season (April 2010), summer monsoon (July 2010) and post monsoon (December 2010). Dissolved cations were measured by Atomic Absorption Spectroscopy at Geosciences Environment Toulouse and DSi was determined by spectrophotometry (Molybdate blue method) at the Indo-French Cell for Water Sciences (IRD-IISc, Bangalore). The sample collection procedures and details about chemical analyses (dissolved load concentration) are described in Meunier et al. (2015) for Kaveri basin and in Gurumurthy et al. (2012) for Netravathi basin. Typical precision for cation

Table 1
Main characteristics of the two river basins (from Gurumurthy et al., 2012 for Netravathi and Meunier et al., 2015 for Kaveri).

	Netravathi	Kaveri
River length (km)	147	765
Location of spring	Western Ghats	Western Ghats
Watershed area (km^2)	3657	85,626
Flow direction	South-west into Arabian Sea	South-east into Bay of Bengal
Net annual discharge ($km^3\ yr^{-1}$)	12 (94% from SW monsoon)	4.5 (mainly SW monsoon and partially from NE monsoon)
Climate	Tropical humid	Tropical humid to semi-arid
Annual rainfall ($mm.yr^{-1}$)	3600-4200	6000 in the Western Ghats to 300 in the East part of Karnataka Plateau
Theoretical runoff ($mm.yr^{-1}$)	3300	260
Land use	51% agricultural land, 35% forest	66% agricultural land, 20% forest
Number of dams	9	96
Population density	397 km^{-2}	1500 km^{-2}
Lithology	Gneiss, metasediments, charnockites	Gneiss, charnockites and granitic rocks + Cretaceous deposits and Quaternary alluvium in lower reaches

concentration were better than 10%. We analysed certified reference material (PERADE-09, Environment Canada) for DSi measurements along with samples which showed a reproducibility of 97.4%. Finally, we verified before the isotopic analysis that the DSi concentration remained stable over time by further DSi measurements at LOCEAN-IPSL.

2.3.2. Si isotopes measurement

The Si fraction was separated from sample matrix with a 2-steps procedure carried out by adapting the protocol MAGIC- MAGnesium Co-precipitation technique (Karl and Tien, 1992; Reynolds et al., 2006; Hughes et al., 2011). After adding $MgCl_2$ to the river water samples to match the seawater Mg concentration, samples were treated with 2% (*v*/v) of 1M NaOH. The brucite $Mg(OH)_2$ formed at high pH scavenges Si which gets adsorbed onto precipitated brucite. The brucite was separated from the supernatant by centrifugation and redissolved in 1 M HCl. The supernatant from the first step was then subjected to second addition of 1% NaOH following the same step. The second brucite precipitate was also redissolved with 1 M HCl and merged with the previous one. The DSi concentration of the dissolved brucite and supernatant was analysed by spectrophotometer (Grasshoff et al., 1999). We verified that the yield of the MAGIC precipitation was 100% by testing the absence of DSi in the second supernatant.

Si purification was carried out using cation exchange resin (BioRad cation exchange resin DOWEX 50 W-X12, 200 to 400 mesh, in H^+ form) following the procedure of Georg et al. (2006a, 2006b). The procedure blank values are monitored continuously and were below 1% of the main signal, i.e. they were considered as negligible. After the purification process, an aliquot was analysed for major elements analysis (Na, Mg, Ca, Al) by ICP-MS (Agilent 7500a) to ensure that the Si/X cations weight ratio is always >50 and then minimize the matrix effects in the plasma. The potential matrix effect resulting mainly from Cl^- and SO_4^{2-} was corrected by the artificial doping of anions (Suprapur H_2SO_4 and HCl) in all the samples and standards (Hughes et al., 2011). The isotopic measurements, 60 cycles of 4 s each, were performed on MC-ICP-MS Neptune+ (LSCE-IPSL, Gif-sur-Yvette) in dry plasma mode with Mg doping as described by Closset et al. (2016) (Table S1 for details). During the isotopic measurements, rinsing solution blanks were measured between each sample standard, and then subtracted. Our method has been intercalibrated for sea water in GEOTRACES measurements (Grasse et al., 2017). $\delta^{30}Si$ is expressed relative to the standard (NBS28) as;

$$\delta^{30}Si\ (‰) = \left(\left({}^{30}Si/{}^{28}Si \right)_{sample} \Big/ \left({}^{30}Si/{}^{28}Si \right)_{standard} - 1 \right) * 1000$$

The analytical precision and accuracy were monitored by the long-term measurements of secondary reference material Diatomite every ten samples. The reproducibility of the measurements was calculated using the standard deviation of 40 standard analyses over one-year measurements ($\delta^{30}Si = +1.28 \pm 0.1‰$, $\delta^{29}Si = +0.65 \pm 0.08‰$, 2SD). They are well in agreement with the consensus isotopic composition of diatomite ($\delta^{30}Si = +1.26 \pm 0.2‰$, $\delta^{29}Si = +0.64 \pm 0.14‰$, 2SD; Reynolds et al., 2007). Due to insufficient volume of samples, the Si isotopic data of the river waters could not be replicated. However, we checked the reproducibility of Si isotopic analyses during the same period on 43 Indian estuarine water samples that have been fully replicated. The average reproducibility on $\delta^{30}Si$ is ±0.2‰ (±2 SD).

Table 2
Si isotopes, DSi and dissolved cations (*atmospheric contribution corrected) and R_e index measured in the Kaveri River basin during dry and wet periods, respectively. Dissolved cations and R_e are from Meunier et al. (2015).

Kaveri	$\delta^{30}Si_{DSi}$	Std. Err.	DSi	Na*	Ca*	K*	Mg*	R_e
	‰		μM					
Dry season reservoirs								
Hemavathi dam	2.1	0.05	208	90	211	28	114	2.0
KRS dam	n.m.	n.m.	309	432	596	30	518	2.4
Nugu dam	2.8	0.04	231	107	234	55	147	2.1
Kabini Dam	1.9	0.05	234	76	165	26	107	1.8
Mettur dam	2.4	0.06	296	621	460	44	527	2.8
River + tributaries								
Kodlipet	1.9	0.04	352	116	139	40	118	1.8
Krishnarajpet	2.2	0.05	232	109	292	33	165	2.0
Nanjangad	1.9	0.05	320	269	481	29	404	2.2
Bannur	2.1	0.04	362	360	890	43	603	2.2
Shinavas falls	1.8	0.07	393	475	600	29	557	2.4
Shimsha river/ Halaguru	2.1	0.05	697	2266	423	79	801	3.7
Arkavathi river/ Sangam	2.4	0.04	602	791	839	86	689	2.5
Hogenekhal falls	1.9	0.05	427	557	594	30	612	2.4
Musiri	2.4	0.17	397	486	416	57	481	2.5
Cholapuram	2.7	0.05	393	415	656	86	553	2.4
Wet season reservoirs								
Hemavathi dam	1.6	0.04	159	142	149	35	81	2.6
KRS dam	1.2	0.04	160	56	185	27	92	1.9
Nugu dam	2.2	0.04	227	69	182	60	109	2.0
Kabini Dam	n.m.	n.m.	131	14	85	26	41	1.5
Mettur dam	1.5	0.04	198	264	353	38	280	2.5
River + tributaries								
Kodlipet	0.3	0.05	145	21	55	12	34	1.1
Krishnarajpet	1.1	0.05	153	32	119	30	62	1.8
Nanjangad	0.8	0.04	158	21	89	25	46	1.5
Bannur	0.5	0.04	172	49	190	24	91	1.8
Shinavas falls	0.8	0.04	176	49	281	25	86	1.9
Shimsha river/ Halaguru	2.6	0.01	540	2270	531	87	850	3.7
Arkavathi river/ Sangam	0.8	0.04	191	92	244	30	128	2.1
Hogenekhal falls	0.9	0.03	260	106	261	34	136	2.0
Musiri	n.m.	n.m.	n.m.	352	507	52	328	2.8
Cholapuram	1.7	0.01	246	298	473	48	300	2.4

n.m.: not measured.

3. Results

3.1. Dissolved silicon and cations

The DSi concentrations for Kaveri and Netravathi water samples are provided in Tables 2 and 3, respectively. Though the origin of both rivers is Western Ghats, the DSi concentrations of the Kaveri river basins was significantly higher than Netravathi irrespective of the seasons ($p = 0.002$). DSi values in the Netravathi and in the upstream Kaveri with its tributaries in the Western Ghats are similar but fluctuate with the seasons. DSi concentration within main stream (Fig. 2a) samples in Kaveri are homogenous with 365 ± 63 μM and 192 ± 48 μM during dry and wet seasons respectively and exhibits significantly higher DSi during dry season ($p < 0.001$). The DSi concentration of tributaries Hemavathi and Kabini are comparable to the mainstream for both seasons. DSi of tributaries Shimsha and Arkavathi are almost two times higher than the mainstream during dry period but only Shimsha showed similar high DSi during wet season (Fig. 2a). Kaveri reservoirs also showed significant seasonal variation during dry and wet periods (256 ± 44 and 175 ± 38 μM, respectively, $p = 0.01$) with lower DSi concentration than the main stream during dry period and similar concentration as mainstream during wet period.

In Netravathi – similar to Kaveri, the DSi concentrations within main stream (Fig. 2b) samples are homogenous with 250 ± 39 μM, 169 ± 22 μM and 151 ± 23 μM during dry, wet, and post-monsoon periods, respectively. The concentrations are significantly different between dry and wet periods of the main stream ($p = 0.02$). The Gurupur river exhibits contrasting DSi concentration compared to Netravathi during all seasons likely because it is only draining the lowland area (Table 3, Fig. 2b). In contrast, the other tributaries exhibit similar concentrations to the mainstream during dry, wet and post monsoon seasons (230 ± 46, 158 ± 16 and 161 ± 10 μM, respectively). Except for the seasonal difference, DSi appears to be relatively homogenous over the entire basin.

In order to assess the contribution of bedrock weathering to the flux exported by the river, cations concentrations were corrected from atmospheric deposits. This approach assumes a negligible contribution of KCl fertilizer and evaporite rocks to the riverine Cl as already discussed in Gurumurthy et al. (2012) and Meunier et al. (2015). The absence of evaporite in these river basins is attested by the pure magmatic origin of their bedrocks. KCl is however applied as fertilizer in Indian agriculture, like in many other countries. Enquiries of fertilizer consumption at Indian states level indicate that the amount of Cl annually brought by fertilizers remains minor compared to the Cl brought by atmospheric inputs (particularly in high rainfall areas). This broad balance in favour of atmospheric sources at large scale does not prevent from observing locally a significant influence of fertilizers on the composition of water, as for example in the groundwater of Kaveri middle reaches (Buvaneshwari et al., 2020). Locally and particularly when a stream is fed by groundwater in an intensive agricultural area, the proportion of anthropogenic Cl may dominate. In absence of specific geochemical signature of anthropogenic Cl, it is not possible to quantify this excess and correct its influence. In this case, the Cl-atmospheric correction is overestimated but to an unknown extent. The good agreement between Na/Cl ratio of rain and seawater has been documented in Netravathi by Gurumurthy et al. (2012). The atmospheric corrected major cations (indicated by *), already published by Meunier et al. (2015) for the Kaveri, are mentioned in Table 2. Those calculated for Netravathi are given in Table 3. The average total dissolved cation concentrations (ΣC^{+}*) of the Kaveri basin are 1417 ± 876 μM and 717 ± 902 μM during dry and wet seasons respectively and for Netravathi, 299 ± 58, 143 ±

Table 3
Si isotopes, DSi and dissolved cations (*atmospheric contribution corrected) measured in the Netravathi river basin during dry, wet and post monsoon period (Data from Gurumurthy et al., 2012).

Netravathi		$\delta^{30}Si_{DSi}$	Std. Err.	DSi	Na*	Ca*	K*	Mg*	R_e
		‰				μM			
Dry season									
N2	Mugeru	1.6	0.04	220	115	109	41	63	2.3
Sha	Shanthimageru	n.m.	n.m.	240	101	98	40	89	2.1
Gun	Gundyahole	1.7	0.04	268	115	111	43	86	2.1
Shi	Shishilahole	0.5	0.03	163	58	55	21	33	1.9
Ner	Neriyahole	1.4	0.04	250	111	78	26	61	2.1
N3	Dharmasthala	n.m.	n.m.	232	112	103	31	54	2.2
N4	Mundaje Hole	1.5	0.04	307	146	98	25	58	2.1
Gur	Gurupura River	n.m.	n.m.	166	99	108	36	64	2.4
Wet Season-Monsoon									
N1	Bantwal BC Road	0.8	0.04	169	36	48	18	31	1.3
N2	Mugeru	0.6	0.05	155	46	54	16	32	1.7
Sha	Shanthimageru	0.5	0.06	141	34	48	16	35	1.5
Gun	Gundyahole	n.m.	n.m.	147	35	46	15	34	1.4
Shi	Shishilahole	0.5	0.07	170	42	52	14	36	1.4
Ner	Neriyahole	0.4	0.06	173	53	49	13	34	1.5
N3	Dharmasthala	0.7	0.09	182	55	63	15	37	1.6
N4	Mundaje Hole	0.9	0.09	198	64	60	15	37	1.6
Gur	Gurupura River	0.4	0.04	389	26	40	14	19	−2.2[#]
Post monsoon									
N2	Mugeru	1.0	0.03	160	94	77	17	58	2.3
Sha	Shanthimageru	1.2	0.05	176	66	65	15	64	1.8
Gun	Gundyahole	1.1	0.03	159	100	73	17	71	2.3
Shi	Shishilahole	1.2	0.03	153	82	68	14	74	2.1
Ner	Neriyahole	n.m.	n.m.	158	74	65	14	72	2.0
N3	Dharmasthala	n.m.	n.m.	144	116	88	18	56	2.6
N4	Mundaje Hole	1.5	0.03	122	107	82	16	57	2.6
Gur	Gurupura River	1.2	0.03	249	63	69	18	46	1.3

n.m.: not measured.
#: Please note that the Re calculation in Gurupura river during monsoon is negative due to overestimation of the atmospheric input and was removed from subsequent figures.

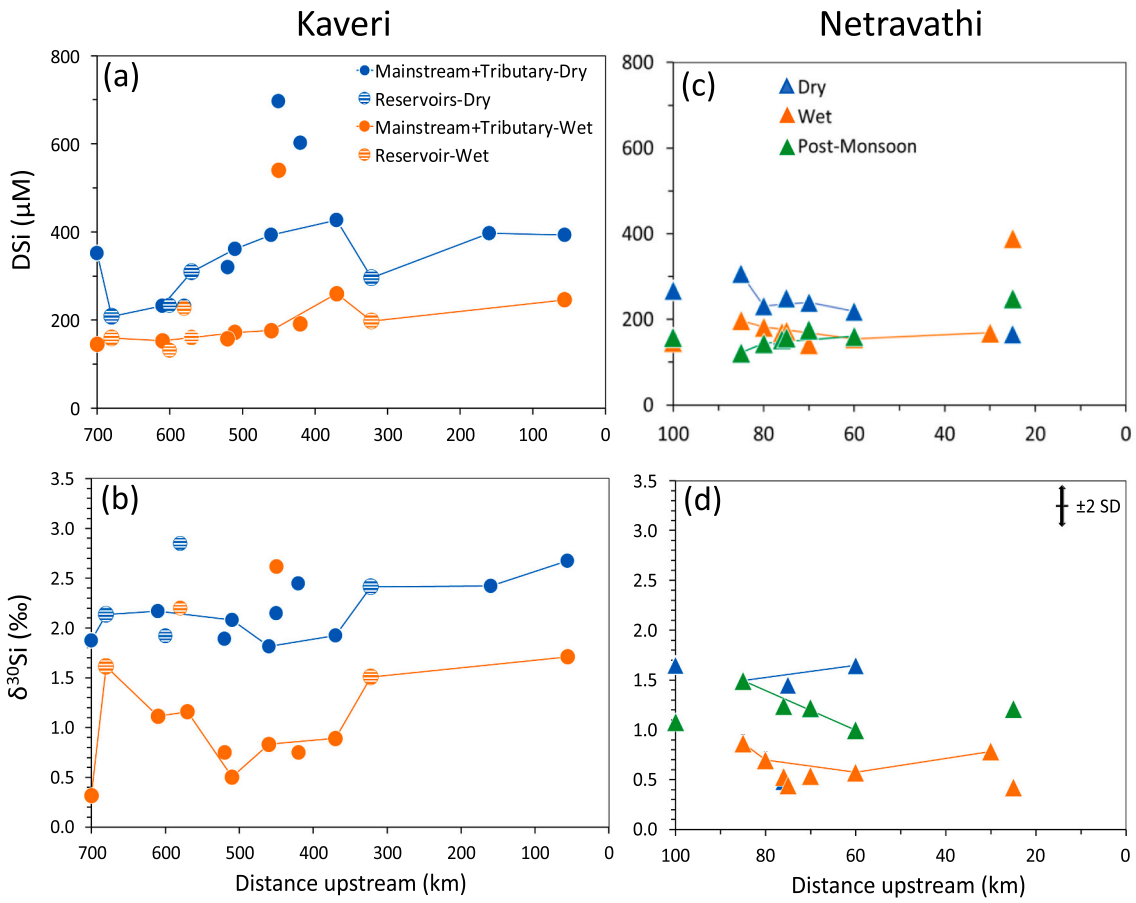

Fig. 2. Spatial and seasonal variability of dissolved Si (DSi) and silicon isotopes of DSi ($\delta^{30}Si_{DSi}$) in the Kaveri (2a, 2b) and Netravathi (2c, 2d) river basins during dry (blue) and wet (orange) periods. Post-monsoon data is available also for Netravathi (green). Water flow is from left to right. The filled circles in Kaveri represent the mainstream and tributaries, and the circle with patterns represent the dams/reservoir (Table 1 for more details). The samples along the mainstream are connected with lines. (For interpretation of the references to colour in this figure legend, the reader is referred to the web version of this article.)

23 µM and 239 ± 28 µM during dry, wet and post monsoon seasons, respectively. ΣC^{+} * was higher in Kaveri compared to Netravathi during both seasons, with the solutes of both basins being less concentrated during wet period. It is also notable that the ΣC^{+} * of the mainstream and tributaries of Kaveri basin tend to increase towards the lower reaches during both seasons (more intensely during dry season) and exceptionally very high concentrations in Shimsa for both seasons and Arkavathi for dry season. In contrast, the ΣC^{+}* in Netravathi tend to be similar in the entire basin during all seasons except Shishilahole of dry period.

3.2. Weathering index

The proxy of silicate weathering degree based on river water geochemistry, molar ratio R_e, originally proposed by Tardy (1971) and modified by Boeglin and Probst (1998), has been calculated by Gurumurthy et al. (2012) for the Netravathi and by Meunier et al. (2015) for the Kaveri. This ratio is based on the concentrations of cations and silicon resulting from silicate weathering in river water.

$$R_e = \frac{\left(3Na^{+} + 3\,K^{+} + 1.25Mg^{2+} + 2Ca^{2+} - DSi\right)}{\left(0.5\,Na^{+} + 0.5\,K^{+} + 0.75\,Mg^{2+} + Ca^{2+}\right)} \quad (1)$$

The coefficients used in the above formula correspond to an average granite containing feldspar, mica, and Mg-silicate minerals such as amphiboles. If the $R_e = 0$, the weathering is intense and forms gibbsite (allitization), if $R_e = 2$, kaolinite is essentially formed (monosiallitization), if $R_e = 4$, the weathering products are mainly smectites (bisiallitization). R_e indeed reflects the molar ratio (SiO_2/Al_2O_3) of the secondary minerals formed in the weathering profile (Tardy, 1971).

The R_e calculated for Kaveri basin ranges from 1.77 to 3.73 (2.35 ± 0.47) and 1.09 to 3.76 (2.10 ± 0.62) during dry and wet periods, respectively (Meunier et al., 2015). The most downstream values measured at Kollidam, which can be considered as integrative of the whole river basin, were 2.36 and 2.43 respectively. Shimsha showed the relatively high R_e value of 3.73 and 3.69 respectively. In Netravathi, R_e ranges from 1.9 to 2.4, 1.3 to 1.7 and 1.3 to 2.6 during dry, wet and post monsoon respectively (Gurumurthy et al., 2012 and Table. 2). There is a significant seasonal difference of R_e between dry and wet periods with significantly lower R_e during wet period compared to dry period ($p < 0.001$).

3.3. Silicon isotopes

The Si isotope compositions of Kaveri and Netravathi river basins are given in Tables 2 and 3. All the samples of Kaveri and Netravathi basins carry a positive value of $\delta^{30}Si_{DSi}$ within the range of recent global river water compilation (Frings et al., 2016 and the references within). The average $\delta^{30}Si_{DSi}$ of the river Kaveri (+1.73 ± 0.71‰) is ~0.7‰ heavier than the Netravathi basin (+0.99 ± 0.43‰) (Fig. 2c and d). The $\delta^{30}Si_{DSi}$ of the Kaveri and Netravathi basins are well comparable with large river basins: +0.9 ± 0.4‰ for Congo basin (Cardinal et al., 2010; Hughes et al., 2011); +1.0 ± 0.6‰ for Amazon basin (Hughes et al., 2013); +1.3 ± 0.5‰ for Yellow river (Ding et al., 2011); +1.5 ± 0.5‰ for Ganges-Brahmaputra basin (Fontorbe et al., 2013; Frings et al., 2015); +1.6 ± 0.4‰ for Tana basin, Kenya (Hughes et al., 2012); +2.1 ± 0.7‰ for Yangtze basin (Ding et al., 2004), while the world river (non-weighted)

average has been estimated to be +1.28 ± 0.7‰ (Frings et al., 2016). Kaveri basin signature is heavier than most global river basins but similar to Ganges-Brahmaputra and Tana basins whereas Netravathi is closer to the humid tropical basins, notably large and mostly pristine Amazon, and Congo basins. In Kaveri basin, seasonal influence is well evidenced between dry (base flow, +2.2 ± 0.3‰) and wet (high flow, +1.2 ± 0.7‰) seasons with a + 1‰ heavier $\delta^{30}Si_{DSi}$ during dry period (Fig. 2c). Noteworthy, there is no significant variability of silicon isotopes between reservoirs, tributaries, and mainstream during dry and wet period, except Nugu dam where the heaviest isotopic composition was measured during dry period (Table 1 and Fig. 2c). Like Kaveri basin, Netravathi also shows a significant seasonal difference in $\delta^{30}Si_{DSi}$ but no significant spatial heterogeneity within the river basin, except the light composition of Shishilahole tributary during dry period (Table 2 and Fig. 2d).

Discharge weighed Si isotopic composition delivered to the estuary by both rivers are calculated using the silicon isotopic signatures and DSi for both dry and wet seasons from the most downstream stations of Kaveri and Netravathi. The data for sampling discharge and DSi flux calculation of Netravathi (1.5 and 9.5 km^3 for dry and wet period discharge) and Kaveri (4.3 and 17 km^3 for dry and wet period discharge) was obtained from Mangalaa et al. (2017) and Meunier et al. (2015) respectively. The weighted $\delta^{30}Si$ signature of DSi exported to the Kaveri estuary is estimated at +1.98‰ which is heavier than the world average (around +0.74‰, Frings et al., 2016) while the $\delta^{30}Si$ signature of DSi exported to the Netravathi estuary is estimated to be +0.93‰, highlighting the contrasted weathering conditions and other factors prevailing in the two watersheds.

4. Discussion

Riverine DSi shows enrichment in heavier isotope of Si relative to the mean continental crust and lies within the range of world rivers reported so far (−0.1‰ up to +3.4‰; Frings et al., 2016; Sutton et al., 2018). Enriched $\delta^{30}Si_{DSi}$ signatures in river water generally result from two main processes: silicate weathering in the regolith resulting in secondary clay mineral formation and, biological uptake. Biological uptake can be of plant uptake from soil porewater, diatom uptake in rivers and streams, also human induced through irrigated agriculture (diversion of surface or ground water, with further release of Si-depleted water by return flow from the paddy fields) and diatom growth in dams/reservoirs. All processes preferentially incorporate lighter Si isotope resulting in heavy Si isotopic composition of the residual dissolved phase. In the next sections we discuss the respective influences of weathering intensity in silicon isotopic composition of river water according to the contrasted pedoclimatic conditions prevailing in Kaveri and Netravathi basins and the influence of anthropogenic factors.

4.1. Weathering processes

4.1.1. Weathering regimes and seasonality of Si and cations in rivers

Silicate weathering rate (SWR) of Netravathi watershed is among the highest reported for granitic gneiss terrain (42 tons/km^2/yr, Gurumurthy et al., 2012), while the estimated SWR in Kaveri basin is almost 4-fold lower (9.4 tons/km^2/yr at Musiri, Pattanaik et al., 2013), reflecting the contrasting weathering regimes. The Western Ghats receive maximum rainfall from SW monsoon, which accounts for 94% of the flow in Netravathi and almost 80% of the total annual flow in the upper reaches of the Kaveri River (Gurumurthy et al., 2012; Pattanaik et al., 2013). In both Kaveri and Netravathi, we observe broad positive and significant correlations between $\delta^{30}Si_{DSi}$, DSi and $\Sigma C^{+}*$ concentrations (Fig. 3a, b, Fig. S1) indicating that $\delta^{30}Si_{DSi}$ compositions are significantly controlled by weathering intensity and clay mineral formation in both river basins. However, the overall positive correlation

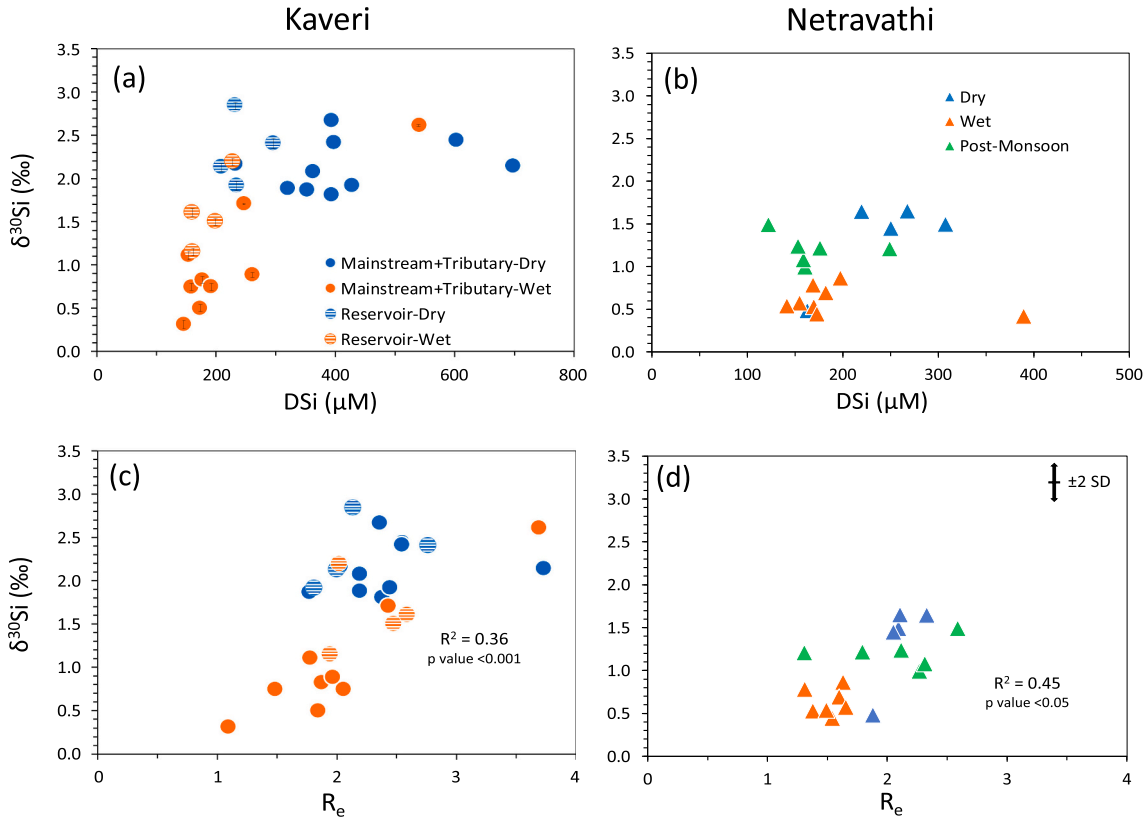

Fig. 3. Evolution of the isotopic signature ($\delta^{30}Si_{DSi}$) in the river Kaveri and Netravathi during different seasons, with dissolved Si concentration (3a, 3b) and R_e (3c, 3d).

between Si isotopic signature and DSi concentration is also driven by seasonal contrasts with higher DSi and heavier $\delta^{30}Si_{DSi}$ during dry season and lower DSi and lighter $\delta^{30}Si_{DSi}$ during wet season (Fig. 3a and b), while $\delta^{30}Si_{DSi}$ vs. DSi concentration or vs. ΣC^{+}* do not exhibit clear relationship among samples collected from a single season. To look further into weathering processes, we compared $\delta^{30}Si_{DSi}$ with R_e as a proxy for silicate weathering, calculated using cation concentration corrected for atmospheric inputs. Since lithologies of basins encompass gneissic and schist belts in the Netravathi and peninsular gneiss, granitic rocks along with amphibolites in Kaveri, R_e is a more suitable proxy to describe weathering intensity and to compare with other tropical rivers rather than DSi/Na* or DSi/(Na* + K*) (Tables 1 and 2, Fig. S1). Coefficients used in the R_e (Eq. (2)) correspond to an average granitic composition with feldspars, micas, and amphiboles, and do not take into account spatial heterogeneities in bedrock composition within each basin. However, it is considered that tributaries and mainstream at least partly average this heterogeneity, which is consistent with good relationship between R_e and DSi/Na* ratio (Fig. S1, Tables 1 and 2).

Seasonal changes in river water geochemistry in Netravathi and Kaveri is affected by monsoon intensity and differences in water-rock interactions within the regolith (weathered rock also named saprolite, and topsoil) and at the weathering front with the fresh bedrock. Given that clay mineral form over months to millennia from metastable amorphous phases (Thiry, 2000), the seasonal changes in the R_e can be attributed to differences in soil-water interaction depths from different levels of the weathering profile leached, i.e., topsoil, saprolite or weathering front (Schaller et al., 2021). The upper range of the relationship between $\delta^{30}Si_{DSi}$ and R_e, heavy Si isotopic signature and high R_e corresponding to the dry period, shows that weathering leachates measured in the river results from smectite formation environment (bisiallitization). By contrast, the lower range of the relationship with lighter Si isotopic signature and low R_e, corresponding to monsoon period, tends to release dissolved elements leached out from a weathering environment where kaolinite-gibbsite formation dominates (monosiallitization and allitization; Fig. 3b, d). However, the stability of minerals can change seasonally depending on the chemical composition of the soil solution and temperature (Zabowski and Ugolini, 1992). In our case, during dry season in both basins, the river base flow is sustained by groundwater, i.e., water that interacted for a long duration while percolating through the thick weathering profile (Mukherjee et al., 2015) down to fresh bedrock minerals at the weathering front, allowing efficient cation and DSi leaching. During monsoon, the rainwater percolates predominantly in surface and subsurface depths with only cation-depleted primary minerals (such as quartz) or secondary minerals (such as kaolinite) in the saprolite and soil, recording a more intense weathering signature (Fig. 3). Seasonal changes of Si isotopic compositions and weathering intensity in these two basins could be defined by the type and duration of water-soil-rock interactions i.e., contributions in various proportions of surface and subsurface flows from different depths as schematically summarised in Fig. 4. Overall, R_e values are lower for Netravathi compared to Kaveri, in line with the more intense weathering fluxes exported by the west flowing river and with the thick lateritic profiles developed in Western Ghats. Intense runoff (3300 mm/yr in Netravathi basin, Gurumurthy et al., 2012) enhances weathering intensity, resulting over long timescales to weathering profiles dominated by kaolinite type clays and iron aluminium oxyhydroxides mineral assemblages (Deepthy and Balakrishnan, 2005). In contrast, Kaveri on the eastern side has shallower and immature weathering profiles characterized by much more complex clay mineral assemblages with both 2:1 clay such as smectites and 1:1 clay such as kaolinites together with residual primary minerals (Deepthy and Balakrishnan, 2005).

4.1.2. *Theoretical framework to understand weathering controls of $\delta^{30}Si_{DSi}$*

Determining how much of the silicon isotopic signature of rivers comes from weathering or biological processes is not trivial because in a watershed both processes are involved to varying degrees depending on the environment. It is often considered that plant Si removal at steady state, has no impact on dissolved fluxes (Cornelis et al., 2011). However, in anthropized hydrosystems, the effects of irrigated agriculture and dams on these fluxes and their isotopic signatures remain difficult to estimate. At the soil-plant scale the contribution of specific silicate

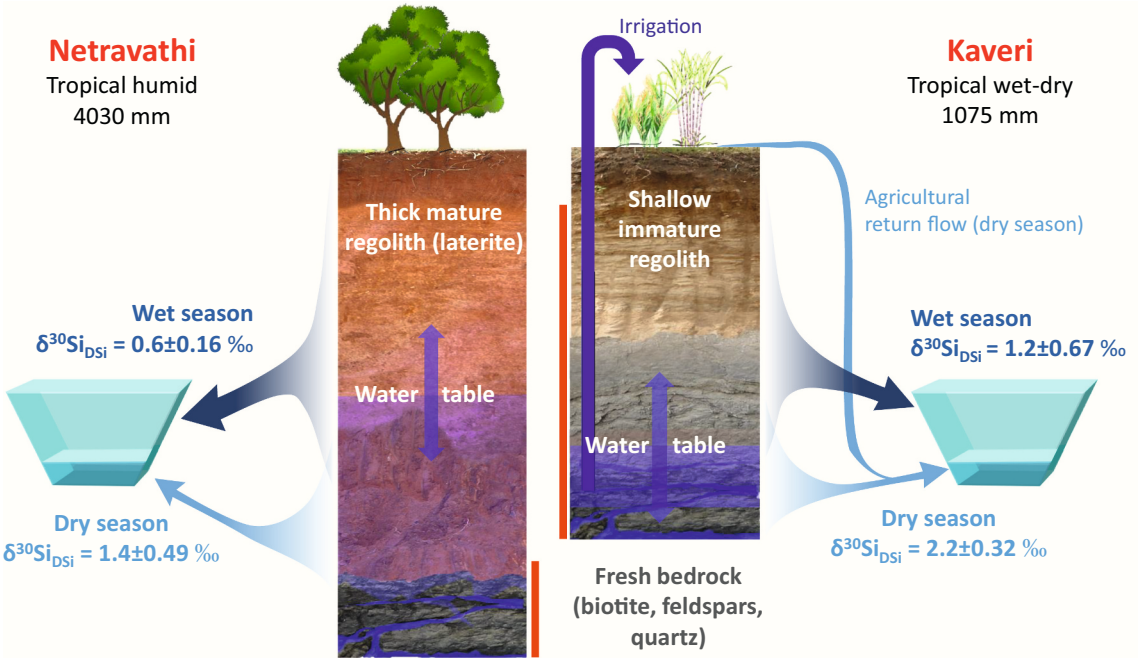

Fig. 4. A schematic of the results from the current study comparing the silicon cycling from two contrasting watersheds in South India. Red bars refer to the section of weathering profile where cation bearing (Na^+, K^+, etc.) primary minerals are still present and are leached. Please note that the weathering profile given is just a representative for middle/lower reaches of Kaveri, the humid high elevation profile in Western Ghats is similar to Netravathi (Deepthy and Balakrishnan, 2005; Braun et al., 2009; Gurumurthy et al., 2012; Meunier et al., 2015).

minerals on $\delta^{30}Si_{DSi}$ can be estimated by combining chemical fluxes and a theoretical isotopic balance, e.g., plagioclase weathering and kaolinite formation from sodium flux and $\delta^{30}Si$ signatures of source rock and clays (Riotte et al. 2018). Such isotope budgets have recently also been proposed for other ubiquitous silicates (Frings et al., 2021). At the scale of a tropical watershed, however, the intense weathering conditions and large spatial scale allow an alternative approach to estimate $\delta^{30}Si_{DSi}$ resulting from weathering of silicate rocks as a function of weathering conditions. This approach is not based on individual minerals that would each be transformed into different clays according to their Si, Al, and cation content, but rather makes the more realistic assumption that all the primary weatherable minerals are weathered and contribute to the formation of secondary phases by releasing silicon and cations within the weathering profile. The isotopic balance is thus carried out by considering; (1) the bulk elemental composition of the gneiss bedrock but removing the fraction of Si and Al in minerals resistant to weathering (quartz, zircon, muscovite/sericite), (2) that the production of secondary minerals is constrained by the Al content of all the weatherable minerals, (3) that the fraction of silicon released in solution and eventually to the river is a function of the type of secondary minerals formed, i.e. of the number of Si atoms allocated in each clay mineral thereafter referred to R_{theo}. This R_{theo} indeed corresponds to the theoretical meaning of R_e: gibbsite (0: no Si incorporated, i.e., allitization), kaolinite (2: two Si incorporated per mole of kaolinite, i.e., monosiallitization) or smectite (4: four Si incorporated per mole of smectite, i.e., bisiallitization) formations (see Eqs. (4) and (6) and details given in Table 4). This conceptual model allows to compare the evolution of the theoretical R_{theo} and the $\delta^{30}Si_{DSi}$ deduced from the isotopic balance. We used the equations below to calculate the fraction of silicon immobilized as clays ($f_{Si\text{-}clay}$), the fraction of silicon released as dissolved silicon ($f_{Si\text{-}DSi}$) and the resulting silicon isotopic composition of dissolved silicon ($\delta^{30}Si_{DSi}$).

$$f_{Si-DSi} + f_{Si-clay} = 1 \quad (2)$$

$$\delta^{30}Si_{DSi} = \frac{\left(\delta^{30}Si_{bedrock} - f_{Si-clay} * \delta^{30}Si_{clay}\right)}{f_{Si-DSi}} \quad (3)$$

For R_{theo} between 0 and 2 secondary minerals formed in soil are only gibbsite and kaolinite and $f_{gibbsite} + f_{kaolinite} = 1$ and;

$$R_{theo} = 2 * f_{kaolinite} \quad (4)$$

$$f_{Si-clay} = Al_{normalized} * f_{gibbsite} * (Si/Al)_{gibbsite} + Al_{normalized} * f_{kaolinite} * (Si/Al)_{kaolinite} \quad (5)$$

For R_{theo} between 2 and 3 secondary minerals formed in soil are only kaolinite and smectite $f_{smectite} + f_{kaolinite} = 1$ and;

$$R_{theo} = 2 * f_{kaolinite} + 4 * f_{smectite} \quad (6)$$

$$f_{Si-clay} = Al_{normalized} * f_{kaolinite} * (Si/Al)_{kaolinite} + Al_{normalized} * f_{smectite} * (Si/Al)_{smectite} \quad (7)$$

Here $f_{gibbsite}$, $f_{kaolinite}$ and $f_{smectite}$ are the proportion of gibbsite, kaolinite and smectite formed during weathering. In Eqs. (5) and (7), Al is normalized to silicon from the chemical and mineralogical composition of the gneiss as source rock, proposed by Braun et al. (2009) for Mule Hole (in the Western Ghats, part of the upper Kaveri basin) and Si/Al ratio of clay types are based on stoichiometry (Table 4). $\delta^{30}Si$ composition of the bedrock (−0.34‰) and clay fraction (−1.3‰) reported in Riotte et al. (2018a, 2018b) from the Kaveri basin are used for $\delta^{30}Si_{bedrock}$ and $\delta^{30}Si_{clay}$ (details of the bedrock composition, secondary product and $\delta^{30}Si$ value ranges are given in Table 4, Table 5).

Since the isotopic balance is strongly dependent on the $\delta^{30}Si$ of the secondary phase, in Eq. (3) we considered both the extreme values published in the literature for $\delta^{30}Si_{clays}$ (−2.1‰ in humid tropics of Sri Lanka comparable to Netravathi and $\delta^{30}Si$ of −0.5‰ for smectite type clays which is lighter than the bedrock; Frings et al., 2021; Georg et al., 2009), along with value measured in kaolinite dominated clay fraction from Mule Hole soils of Kaveri basin (−1.3‰; Riotte et al., 2018a, 2018b) (Fig. 5). The evolution of $\delta^{30}Si$ as a function of R_{theo} is considered robust between 0 and 2 because the conditions for intense weathering are met (Table 5). On the other hand, R_{theo} beyond 2 corresponds to progressive formation of smectite type clays with lower intensity of weathering, which is consistent with the observation that a part of the weatherable primary minerals is still present in weathering profiles (see e.g., Violette et al., 2010 for Mule Hole). Therefore, the evolution of $\delta^{30}Si$ for R_{theo} between 2 and 3 (still dominant kaolinite formation) is only indicative. For R_{theo} of 0, the $\delta^{30}Si$ corresponds to the signature of the parent rock which is expected as Si is not incorporated into any secondary mineral. $\delta^{30}Si_{DSi}$ then increases with R_{theo} as the silicon immobilized in the clays are lighter in silicon isotopic composition. Thus, at R_{theo} of 2 (kaolinite formation) the maximum $\delta^{30}Si$ of the solute phase is 1.2‰. Beyond 2 the $\delta^{30}Si$ increases up to 5.7‰ which could explain in part certain high $\delta^{30}Si_{DSi}$ signatures of world rivers. Current framework also allows to check the whole rock weathering including the stable minerals such as quartz and sericite, which shows relatively low fractionation in $\delta^{30}Si_{DSi}$ with increasing R_{theo}. Gneiss composition corrected for stable minerals such as quartz and muscovite better represents the measured values in natural river water samples compared to whole rock weathering scenario, indicating negligible Si leaching from the resistant mineral phases (Fig. 5).

In the Netravathi, the spatio-temporal variations of R_e and $\delta^{30}Si$ observed match the theoretical curve defined by the lightest $\delta^{30}Si$ kaolinite formation (−2.1‰ found in humid tropics similar to Netravathi climate) and few samples within $\delta^{30}Si_{clay}$ of −1.3‰. This means that the local or seasonal weathering conditions taking place in this river basin are sufficient to explain the $\delta^{30}Si$ variability in the river system. In

Table 4
The stoichiometric composition and $\delta^{30}Si$ of the bedrock and possible secondary product compositions used to derive the theoretical relationships between $\delta^{30}Si_{DSi}$ and weathering intensity in the river basins ($^{\nabla}$ Braun et al., 2009; $^{\#}$ Opfergelt and Delmelle, 2012; * Frings et al., 2021; $^{\Phi}$ Riotte et al., 2018a, 2018b).

$Bedrock_{initial}$	Secondary product	$\delta^{30}Si_{clay}$	R_{theo}
Whole Gneiss$^{\nabla}$	Gibbsite, $Al(OH)_3$	-	0
$Si_{1.14}Al_{0.27}Ca_{0.04}Mg_{0.06}$ $Na_{0.14}$ $K_{0.04}$	Kaolinite, $Si_2Al_2O_5(OH)_4$	−1 to −2 ‰*	2
$\delta^{30}Si = -0.34‰^{\Phi}$	Smectite $Si_4O_{10}(OH)_2Mg_{0.33}Al_{1.67}Ca_{0.16}$	−0.2 to −1 ‰$^{\#}$	4
Gneiss without quartz and sericite$^{\nabla}$	Gibbsite, $Al(OH)_3$	-	0
$Si_{0.57}Al_{0.26}$ $Ca_{0.04}Mg_{0.06}$ $Na_{0.14}$ $K_{0.02}$	Kaolinite, $Si_2Al_2O_5(OH)_4$	−1 to −2 ‰*	2
$\delta^{30}Si = -0.34‰^{\Phi}$	Smectite $Si_4O_{10}(OH)_2Mg_{0.33}Al_{1.67}Ca_{0.16}$	−0.2 to −1 ‰$^{\#}$	4

Table 5
Calculated values of $\delta^{30}Si_{DSi}$ and theoretical weathering index (R_{theo}) using the equations given in the text. Two scenarios involving either weathering of gneiss with and without quartz and sericite mineral fraction is considered for calculating the evolution of the Rtheo and $\delta^{30}Si_{DSi}$.

$f_{gibbsite}$	$f_{kaolinite}$	$f_{smectite}$	$f_{Si\text{-}clay}$	$f_{Si\text{-}DSi}$	$\delta^{30}Si_{DSi}$	R_{theo}
Weathering of gneiss without quartz and sericite						
1	0	0	0.00	1.00	−0.34	0
0.5	0.5	0	0.23	0.77	−0.06	1
0	1	0	0.45	0.55	0.46	2
0	0.5	0.5	0.77	0.23	2.90	3
Weathering of whole gneiss						
1	0	0	0.00	1.00	−0.34	0
0.5	0.5	0	0.12	0.88	−0.21	1
0	1	0	0.24	0.76	−0.04	2
0	0.5	0.5	0.40	0.60	0.30	3

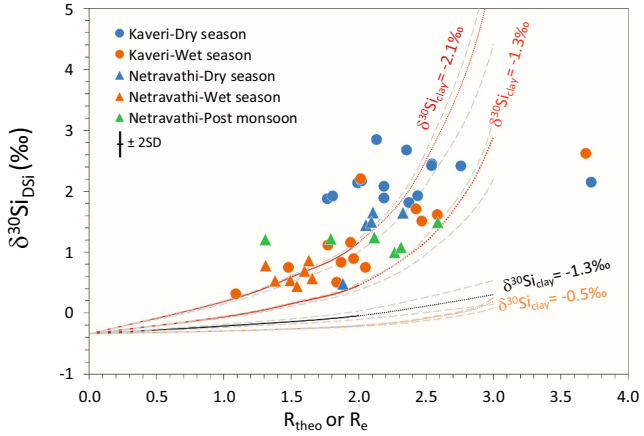

Fig. 5. The evolution of R_{theo} and $\delta^{30}Si_{DSi}$ as rock weathers and transforms into secondary products plotted along with measured R_e of river water samples from Kaveri and Netravathi. Trendline for three different silicon isotopic compositions for the clay is plotted for the gneiss weathering corrected for quartz and sericite contribution (maroon, red and orange for $\delta^{30}Si_{product}$ values of −2.1‰, −1.3‰ and −0.5‰ respectively). The scenario for whole gneiss weathering and $\delta^{30}Si_{product}$ of −1.3‰ is shown in black. The grey dashed lines represent the sensitivity depending on the deviation in the chemical composition in the intial rock composition (Braun et al., 2009). R_e calculation in Gurupura river is negative due to overestimation of the atmospheric input is not displayed. (For interpretation of the references to colour in this figure legend, the reader is referred to the web version of this article.)

contrast, only few samples from Kaveri tributaries and the mainstream show $\delta^{30}Si_{DSi}$ signatures consistent with theoretical R_{theo} for $\delta^{30}Si_{clay}$ of −1.3‰ (which is observed in Kaveri basin by Riotte et al., 2018a, 2018b). Overall $\delta^{30}Si_{DSi}$ of the Kaveri samples was on average + 0.67 ± 0.4‰ and + 1.34 ± 0.4‰ heavier during wet season and dry season respectively than the theoretical value expected by a single control of silicate weathering with $\delta^{30}Si_{clays}$ of −1.3‰. This discrepancy shows that the heavy $\delta^{30}Si$ signatures observed especially during the dry season can partly be the result of biological and/or anthropogenic processes (see section 4.2 for details).

4.1.3. Comparison with other tropical rivers

Overall, the seasonal variations of major elements as well as of $\delta^{30}Si_{DSi}$ are similar with those of the Amazon basin and tributaries (Hughes et al., 2013) as observed in the $\delta^{30}Si_{DSi}$ vs. R_e index comparison

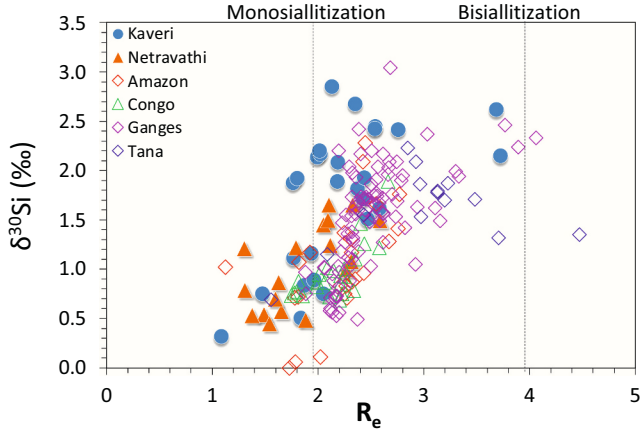

Fig. 6. $\delta^{30}Si_{DSi}$ and R_e of the present study compared with the values from other studies global river water (see text for details, Amazon from Hughes et al. (2013); Congo from Hughes et al. (2011); Tana from Hughes et al. (2012); Ganges from Fontorbe et al. (2013)).

with other tropical rivers (Fig. 6). The range of weathering index in the present study is comparable to the R_e values of other worldwide rivers (discussed in Gurumurthy et al., 2012): Ganges-Brahmaputra (2.2), Amazon (2.1) and Congo-Zaire (2.1) are similar to Kaveri basin, whereas, the Orinoco (1.6), Parana (1.4) and Mekong (1.7) are more comparable to the Netravathi basin. It is also interesting to note from the Fig. 6, that the two contrasted Indian tropical basins with many anthropogenic pressures are behaving similarly as the tributaries and mainstream of the Amazon basin (data from Hughes et al., 2013), Congo river (Hughes et al., 2011), Tana river (Hughes et al., 2012) that are very different in size and type (e.g., with much less anthropogenic impact especially for Congo and Amazon) indicating that silicate weathering remains a major process that controls the Si isotopic variability. Likewise, in Ganges combination of both above mentioned processes control the $\delta^{30}Si_{DSi}$ variability (Fontorbe et al., 2013). Compilation of the R_e and $\delta^{30}Si_{DSi}$ from tropical rivers indicates a broad decrease of $\delta^{30}Si_{DSi}$ with increasing weathering intensity which is consistent with the $\delta^{30}Si$ of soils (Opfergelt and Delmelle, 2012).

4.2. Biotic and anthropogenic impacts

4.2.1. Water use and crops

Vegetation cover and aquatic diatoms can significantly affect Si cycling in surface water by controlling riverine DSi load (Derry et al., 2005; Cornelis et al., 2011). Deforestation and conversion to agricultural field also affect Si cycling by enhancement of erosion and dissolution of amorphous silica (ASi) that increases riverine DSi. Conversely, phytoliths may decrease riverine DSi due to crops harvesting and subsequent removal from the system (Conley et al., 2008). Regarding Si isotopic signatures, more intensive agricultural activities can lead to more incorporation of lighter Si isotopes in the plants, leaving heavier Si isotopic signature in the soil solution (Vandevenne et al., 2012, Riotte et al., 2018a, 2018b) and rivers (Delvaux et al., 2013). Contrasting land use and land cover in Kaveri and Netravathi basins can significantly impact $\delta^{30}Si_{DSi}$ and river water geochemistry. Indeed, Kaveri River basin with higher agricultural land area (almost 66%) show higher $\delta^{30}Si_{DSi}$ compared to the Netravathi during dry season. However, there is also an overlapping signal from the abiotic weathering process arising from these various lithologies, climate and anthropogenic influences in the overall $\delta^{30}Si_{DSi}$ signature. The broad increase in $\delta^{30}Si_{DSi}$ along the Kaveri course could indeed result from the multiple return flows from paddy fields irrigation in command areas (almost 80% of the surface water is deviated for irrigation; Meunier et al., 2015), or from a larger fraction of Si incorporated in the clays of the semi-arid middle and lower reaches. DSi removal in cultivated regions of Kaveri basin where silicon-accumulating crops such as paddy, sugarcane and maize are grown, will be dominated by the plant uptake upon adsorption which fractionates against $^{30}Si_{DSi}$, leading to a heavy isotopic signature in soil solution (Riotte et al., 2018a, 2018b). The primary purpose of the dams and reservoirs in Kaveri is to provide water through canals for irrigating the cultures located downstream each structure (named command areas). The water in excess returns to the main river channel as return flow with a relatively heavier $\delta^{30}Si_{DSi}$ as observed in stagnant water of paddy fields (upto +4.4‰, Riotte et al., 2018b). The contribution of SW monsoon decreases towards lower reaches of Kaveri with Shimsha and Arkavathi watersheds receiving only limited rainfall (Pattanaik et al., 2013). These two tributaries are dammed and the water reaching Kaveri is a mix of sewage, return flow from irrigated agriculture and possible local groundwater contributions. Therefore, the exceptionally heavy isotopic composition at Shimsha river on the lower reach in both seasons (+2.1 and + 2.6‰) and the Arkavathi during dry season (+2.4‰) can result from dissolved Si that has encountered several cycles of isotopic enrichments due to plant uptake combined to evaporation that has increased Si concentration. This is consistent with high total cations and comparable values of major cations during dry and wet seasons of Shimsha river. Such heavy $\delta^{30}Si$ corresponds to return flow from

irrigated agriculture that leaves the residual DSi fraction of these waters, enriched in ^{30}Si (Riotte et al., 2018b). Kaveri river water samples also showed a broad range of Cl concentration with an average of 646 μM for both seasons which is almost 8-fold higher than Netravathi. Such high concentration is likely to result from the combined effect of evapotranspiration, irrigation, and recycling, along with additional inputs from fertilizers such as potash (KCl), which is well documented in an agricultural watershed in Kabini basin (Buvaneshwari et al., 2020). During the wet period, the dilution effect is generally seen in dissolved load concentration, but the contrasted Si isotopic composition cannot be only explained by a dilution process. Si isotopic signature of the mainstream is gradually getting heavier towards the lower reach, while the tributaries and reservoirs exhibit higher variability during wet period (Fig. 2b). Therefore, as discussed in section 4.1.2 and seen in Fig. 5 weathering predominantly controls Si isotope variations in the upper reaches of Kaveri receiving the maximum precipitation while increased contribution of return flow from irrigated agriculture into the mainstream and tributaries leads to an increase in $\delta^{30}Si_{DSi}$ of DSi in the lower reaches of Kaveri.

4.2.2. Amorphous silica (ASi) and dams

The relationship between amorphous silica (ASi) and $\delta^{30}Si_{DSi}$ in rivers suspended matter are not straightforward, as shown by Hughes et al. (2011) in the Congo River, because of the importance of fast diatoms settling in the sediment. According to the only three counting available, the ASi fraction in Kaveri River is constituted half by phytoliths (mainly originating from grass and sedge species) and half by diatom frustules (Meunier et al., 2015), except in reservoir where diatoms largely dominate. In the case of the Kaveri River, we did not observe any correlation between $\delta^{30}Si_{DSi}$ and ASi, indicating increase in ASi fraction, resulting from an increased diatom growth, cannot account for the heavy silicon isotopic compostion (ASi data from Meunier et al., 2015). To check for the role of diatoms in the river basin during dry season, we also used the approach detailed in Hughes et al. (2011) (Appendix A). However, the calculation suggests that the influence of diatom uptake is unlikely to explain the variability of $\delta^{30}Si_{DSi}$ in Kaveri basin during the dry season due to the unrealistic BSi required for such heavy $\delta^{30}Si_{DSi}$ and the lack of any correlation with ASi. Phytoliths are labile Si pools with dissolution rates lower than secondary clay minerals and can be an important contributor to riverine silicon cycling (Fraysse et al., 2009). Previous study from Mule Hole watershed in Kabini basin shows that $\delta^{30}Si$ of soil and suspended load ASi fraction dominated by phytolith varies in a narrow range from +1.1 to +1.4‰ (Riotte et al., 2018a), which are unlikely to explain the heavy silicon isotopic composition during dry season.

Reservoirs and dams increase the residence time of water and favour enhanced diatom growth and accumulation in sediments which cause a decline in DSi downstream the reservoir (Conley et al., 2000; Humborg et al., 2002; Hughes et al., 2012). Meunier et al. (2015) reported a dominance of diatoms in the ASi pool of the Nugu reservoir that may explain decrease of DSi content. Reservoirs in the present study do not show any significant difference in Si concentration or isotopic signature compared to the mainstream and tributaries for both seasons except Nugu reservoir during dry season (+2.8‰, Table 2, Fig. 2 a, c). Nugu reservoir also shows higher ASi (73.8 μM) and low DSi (231 μM) and was reported to have higher diatom abundance (94%) in the ASi fraction relative to the other adjacent reservoirs, clearly indicating increased diatom production leading to higher $\delta^{30}Si_{DSi}$ value of the water (Fig. 2 a, c and Meunier et al., 2015). Using this isotopic composition as the $\delta^{30}Si_0$ and applying Eqs. (a) and (b) in Appendix, gives calculated BSi of 258 μM and 693 μM for Rayleigh and steady state models, respectively. The value obtained by the Rayleigh model is larger but comparable to the highest value calculated in Malebo pool by Hughes et al. (2011) in which 215 μM of DSi has been consumed and appears realistic for diatom production within a tropical lake during summer. However, none of the other Kaveri reservoirs showed enhanced ASi values, which indicate negligible role of biotic uptake at the scale of the Kaveri Basin. During the wet season, higher discharge and turbidity limit diatom growth as clearly shown by the extreme shallowness of photic depth, 0.13 ± 0.1 m, during high discharge in Godavari estuary (Sarma et al., 2009). There are no ASi data measured from Netravathi basin to assess the biological uptake, but comparatively fewer dams in this basin and lighter Si isotopic composition than Kaveri suggest limited impact of biotic process in Si biogeochemical cycling in Netravathi. Kaveri river and its tributaries have been supporting irrigated agriculture in middle and lower reaches for centuries (two millennia in the Kaveri delta) and the dams and reservoirs were primarily built to retain monsoon flow and sustain agriculture through canal irrigation during dry season. Higher extent of cultivation and irrigation with the help of reservoirs and dams can lead to significant DSi removal over time and a heavier isotopic signature for agriculture return flow. Such impacts from biotic uptake can overlap with weathering controls of $\delta^{30}Si_{DSi}$ values in river water spatially and temporally.

5. Conclusions

In this study, we report the first dataset of riverine $\delta^{30}Si_{DSi}$ signatures in the Kaveri and Netravathi River Basins, both originating from the Western Ghats (India) but flowing east and west directions, respectively with contrasting land use and climate. Both basins are seasonally well marked, and the $\delta^{30}Si_{DSi}$ in Kaveri river is ~1‰ heavier than that of Netravathi River. This results in a weighted $\delta^{30}Si_{DSi}$ of DSi exported to estuary more fractionated in Kaveri (+1.98‰) than in Netravathi (+0.93‰). The $\delta^{30}Si_{DSi}$ is mainly controlled by weathering regime and water flow which is in turn driven by the short- and long-term hydrological conditions prevailing in each catchment. The long term explains the thickness and abundance of cation-depleted weathering profiles while the short term seasonal scale explains the different levels of water-rock interaction in the weathering profile. We compare $\delta^{30}Si_{DSi}$ signatures with R_e weathering index based on water cation geochemistry. Low R_e in Netravathi indicates intense weathering with formation of kaolinite-gibbsite in the river basin, while most of the Kaveri basin is dominated by smectite-kaolinite assemblage. Both river basins display similar $\delta^{30}Si_{DSi}$ seasonal pattern, with higher $\delta^{30}Si_{DSi}$ and R_e during dry season resulting from soil water release close to the weathering front (i.e., deep saprolite and bedrock) and lower $\delta^{30}Si_{DSi}$ and lower R_e during wet season due to intense weathering. The weathering index Re calculated for both rivers is comparable to the values of other tropical rivers, for instance the Amazon river and its tributaries. We propose a new conceptual approach based on bedrock element geochemistry and redistribution during weathering of Si into secondary mineral on the one hand and released to dissolved phase on the other hand (R_{theo} directly comparable to R_e), to calculate expected $\delta^{30}Si_{DSi}$ signatures. Comparison between calculated and measured $\delta^{30}Si_{DSi}$ allows to estimate whether river Si isotopic signatures can be fully explained only by weathering or if other processes are involved. In Netravathi basin we show that weathering processes are sufficient to explain the $\delta^{30}Si_{DSi}$ signatures and that anthropogenic pressures have a minor contribution. But in Kaveri we found that the $\delta^{30}Si_{DSi}$ are on average + 0.67 ± 0.4‰ and + 1.34 ± 0.4‰ heavier during wet season and dry season respectively than the expected theoretical curve. We ascribe this offset to canal irrigation downstream major dams during dry season that leads to return flow contribution to the river which increases $\delta^{30}Si_{DSi}$ in the river, leading to overall enriched signature in river water. We also suggest that diatoms Si uptake in the Kaveri stream is generally negligible except in the Nugu reservoir (Kaveri tributary) in dry season. Overall, the present study

emphases the control of climatic conditions the $\delta^{30}Si$ of the studied rivers, through the intensity of silicate weathering and nature of the secondary clays produced. It also quantifies, for the first time, the effect of anthropogenic activities (daming and irrigated agriculture) on the silicon isotopic composition of rivers.

Supplementary data to this article can be found online at https://doi.org/10.1016/j.chemgeo.2022.120883.

Declaration of Competing Interest

The authors declare that they have no known competing financial interests or personal relationships that could have appeared to influence the work reported in this paper.

Acknowledgements

The authors would like to thank M. Benrahmoune (LOCEAN-IPSL) for help in sample processing and clean lab management. This work has been supported by the French National programme EC2CO (BIO-HEFECT) - LEFE (CYBER) managed by INSU-CNRS (project SINDIA). K. R. Mangalaa scholarship has been mainly provided by the Erasmus Mundus Action 2 of the European Union (GATE project), with additional support from the Scientific Department of French Embassy in India and by the European Union Seventh Framework Program under grant agreement #294146 (MuSiCC Marie Skłodowska-Curie Actions CIG). We warmly thank IRD for providing Sarath P.K. Ph.D. scholarship and constant support. The work also benefited from CEFIPRA-IFCPAR support (NUNDERGROUND, project # 5907) and from analyses at ALYSES facility (IRD-SU). We thank the AE Oleg Pokrovsky, Luc André and three anonymous reviewers for their thorough comments that greatly helped to improve this manuscript.

Appendix A. Checking the role of diatoms on $\delta^{30}Si$ composition of river water

Here, we assume that the heavier isotopic composition of Kaveri basin in dry season results from the diatom uptake and the $\delta^{30}Si$ is used as a proxy to quantify the uptake mechanism. Based on our assumption, the production of BSi (biogenic silica) as the only main output of DSi for the given water, then $f_{Si} = DSi/(DSi + BSi)$, and one can rewrite the Rayleigh and Steady state equations as:

$$\text{Rayleigh}: BSi = DSi \times \left[exp\left(\left(\delta^{30}Si_0 - \delta^{30}Si\right)/\varepsilon\right) - 1\right] \quad (a)$$

$$\text{Steady state}: BSi = DSi \times \left[\left(\varepsilon/\delta^{30}Si - \delta^{30}Si_0 + \varepsilon\right) - 1\right] \quad (b)$$

$\delta^{30}Si_0$ is considered as 1.81‰, which is the lightest in the river stream during dry period. The fractionation factor (ε) is −1.2‰ (Fripiat et al., 2011; Alleman et al., 2005; Georg et al., 2006a, 2006b).

Based on both Rayleigh and steady state models, the calculated BSi varied 174 ± 165 and 294 ± 350 μM in the mainstream and tributaries of Kaveri respectively whereas the measured ASi values varied 5.6 ± 8.9 μM (Meunier et al., 2015). Moreover, no relation was observed between measured ASi and calculated BSi. It is not realistic to have such high BSi production by diatoms to explain the isotopic composition in the basin because the residence time of the water in the stream is too short to allow such dense growth of diatoms. Moreover, this mechanism is even true for the reservoirs due to the quick usage of water for irrigation. On contrary, in river Congo, higher stability of water flow made favorable for diatom growth was noticed by Hughes et al. (2011) and that could explain the relationship between Si isotopes and ASi.

References

Alexandre, A., Meunier, J.D., Colin, F., Koud, J.M., 1997. Plant impact on the biogeochemical cycle of silicon and related weathering processes. Geochim. Cosmochim. Acta 61, 677–682.

Alleman, L.Y., Cardinal, D., Cocquyt, C., Plisnier, P.D., Descy, J.P., Kimirei, I., Sinyinza, D., André, L., 2005. Silicon isotopic fractionation in Lake Tanganyika and its main tributaries. J. Great Lakes Res. 31, 509–519.

André, L., Abraham, K., Hofmann, A., Monin, L., Kleinhanns, I.C., Foley, S., 2019. Early continental crust generated by reworking of basalts variably silicified by seawater. Nat. Geosci. 2019 12 (9 12), 769–773. https://doi.org/10.1038/s41561-019-0408-5.

Boeglin, J.L., Probst, J.L., 1998. Physical and chemical weathering rates and CO2 consumption in a tropical lateritic environment: the upper Niger Basin. USDA for. Serv. - Gen. Tech. Rep. RMRS-GTR 148, 137–156.

Braun, J.J., Descloitres, M., Riotte, J., Fleury, S., Barbiéro, L., Boeglin, J.L., Violette, A., Lacarce, E., Ruiz, L., Sekhar, M., Mohan Kumar, M.S., Subramanian, S., Dupré, B., 2009. Regolith mass balance inferred from combined mineralogical, geochemical and geophysical studies: Mule Hole gneissic watershed, South India. Geochim. Cosmochim. Acta 73, 935–961.

Buvaneshwari, S., Riotte, J., Sekhar, M., Sharma, A.K., Helliwell, R., Kumar, M.S.M., Braun, J.J., Ruiz, L., 2020. Potash fertilizer promotes incipient salinization in groundwater irrigated semi-arid agriculture. Sci. Rep. 10, 1–14. Available at: https://doi.org/10.1038/s41598-020-60365-z.

Cardinal, D., Gaillardet, J., Hughes, H.J., Opfergelt, S., André, L., 2010. Contrasting silicon isotope signatures in rivers from the Congo Basin and the specific behaviour of organic-rich waters. Geophys. Res. Lett. 37 (12).

Closset, I., Cardinal, D., Rembauville, M., Thil, F., Blain, S., 2016. Unveiling the Si cycle using isotopes in an iron-fertilized zone of the Southern Ocean: from mixed-layer supply to export. Biogeosciences 13, 6049–6066.

Conley, D.J., 1997. Riverine contribution of biogenic silica to the oceanic silica budget. Limnol. Oceanogr. 42, 774–777.

Conley, D.J., Stålnacke, P., Pitkänen, H., Wilander, A., 2000. The transport and retention of dissolved silicate by rivers in Sweden and Finland. Limnol. Oceanogr. 45, 1850–1853. Available at: http://doi.wiley.com/10.4319/lo.2000.45.8.1850.

Conley, D.J., Humborg, C., Smedberg, E., Rahm, L., Papush, L., Danielsson, Å., Clarke, A., Pastuszak, M., Aigars, J., Ciuffa, D., Mörth, C.M., 2008. Past, present and future state of the biogeochemical Si cycle in the Baltic Sea. J. Mar. Syst. 73, 338–346.

Cornelis, J.T., Delvaux, B., Georg, R.B., Lucas, Y., Ranger, J., Opfergelt, S., 2011. Tracing the origin of dissolved silicon transferred from various soil-plant systems towards rivers: a review. Biogeosciences 8, 89–112.

Deepthy, R., Balakrishnan, S., 2005. Climatic control on clay mineral formation: evidence from weathering profiles developed on either side of the Western Ghats. J. Earth Syst. Sci. 114, 545–556.

Delvaux, C., Cardinal, D., Carbonnel, V., Chou, L., Hughes, H.J., André, L., 2013. Controls on riverine δ30Si signatures in a temperate watershed under high anthropogenic pressure (Scheldt - Belgium). J. Mar. Syst. 128, 40–51.

Derry, L.A., Kurtz, A.C., Ziegler, K., Chadwick, O.A., 2005. Biological control of terrestrial silica cycling and export fluxes to watersheds. Nature 433, 728–731. Available at: www.nature.com/nature.

Ding, T., Wan, D., Wang, C., Zhang, F., 2004. Silicon isotope compositions of dissolved silicon and suspended matter in the Yangtze River, China. Geochim. Cosmochim. Acta 68, 205–216.

Ding, T.P., Gao, J.F., Tian, S.H., Wang, H.B., Li, M., 2011. Silicon isotopic composition of dissolved silicon and suspended particulate matter in the Yellow River, China, with implications for the global silicon cycle. Geochim. Cosmochim. Acta 75, 6672–6689.

Dürr, H.H., Meybeck, M., Hartmann, J., Laruelle, G.G., Roubeix, V., 2011. Global spatial distribution of natural riverine silica inputs to the coastal zone. Biogeosciences 8, 597–620. https://doi.org/10.5194/bg-8-597-2011.

Engström, E., Rodushkin, I., Ingri, J., Baxter, D.C., Ecke, F., Österlund, H., Öhlander, B., 2010. Temporal isotopic variations of dissolved silicon in a pristine boreal river. Chem. Geol. 271, 142–152.

Fontorbe, G., De La Rocha, C.L., Chapman, H.J., Bickle, M.J., 2013. The silicon isotopic composition of the Ganges and its tributaries. Earth Planet. Sci. Lett. 381, 21–30.

Fraysse, F., Pokrovsky, O.S., Schott, J., Meunier, J.D., 2009. Surface chemistry and reactivity of plant phytoliths in aqueous solutions. Chem. Geol. 258, 197–206. https://doi.org/10.1016/J.CHEMGEO.2008.10.003.

Frings, P.J., Clymans, W., Fontorbe, G., Gray, W., Chakrapani, G., Conley, D.J., De La Rocha, C., 2015. Silicate weathering in the Ganges alluvial plain. Earth Planet. Sci. Lett. 427, 136–148.

Frings, P.J., Clymans, W., Fontorbe, G., De La Rocha, C.L., Conley, D.J., 2016. The continental Si cycle and its impact on the ocean Si isotope budget. Chem. Geol. 425, 12–36.
Frings, P.J., Oelze, M., Schubring, F., Frick, D.A., von Blanckenburg, F., 2021. Interpreting silicon isotopes in the Critical Zone. Am. J. Sci. 321, 1164–1203. https://doi.org/10.2475/08.2021.02.
Fripiat, F., Cavagna, A.J., Dehairs, F., Speich, S., André, L., Cardinal, D., 2011. Silicon pool dynamics and biogenic silica export in the Southern Ocean inferred from Si-isotopes. Ocean Sci. 7, 533–547.
Ganasri, B.P., Ramesh, H., 2016. Assessment of soil erosion by RUSLE model using remote sensing and GIS - a case study of Nethravathi Basin. Geosci. Front. 7, 953–961.
Georg, R.B., Reynolds, B.C., Frank, M., Halliday, A.N., 2006a. Mechanisms controlling the silicon isotopic compositions of river waters. Earth Planet. Sci. Lett. 249, 290–306.
Georg, R.B., Reynolds, B.C., Frank, M., Halliday, A.N., 2006b. New sample preparation techniques for the determination of Si isotopic compositions using MC-ICPMS. Chem. Geol. 235, 95–104.
Georg, R.B., Reynolds, B.C., West, A.J., Burton, K.W., Halliday, A.N., 2007. Silicon isotope variations accompanying basalt weathering in Iceland. Earth Planet. Sci. Lett. 261, 476–490.
Georg, R.B., Zhu, C., Reynolds, B.C., Halliday, A.N., 2009. Stable silicon isotopes of groundwater, feldspars, and clay coatings in the Navajo Sandstone aquifer, Black Mesa, Arizona, USA. Geochim. Cosmochim. Acta 73, 2229–2241. https://doi.org/10.1016/J.GCA.2009.02.005.
Grasse, P., Brzezinski, M.A., Cardinal, D., De Souza, G.F., Andersson, P., Closset, I., Cao, Z., Dai, M., Ehlert, C., Estrade, N., François, R., Frank, M., Jiang, G., Jones, J.L., Kooijman, E., Liu, Q., Lu, D., Pahnke, K., Ponzevera, E., Schmitt, M., Sun, X., Sutton, J.N., Thil, F., Weis, D., Wetzel, F., Zhang, A., Zhang, J., Zhang, Z., 2017. GEOTRACES inter-calibration of the stable silicon isotope composition of dissolved silicic acid in seawater. J. Anal. At. Spectrom. 32, 562–578. Available at: https://pubs.rsc.org/en/content/articlehtml/2017/ja/c6ja00302h.
Grasshoff, K., Kremling, K., Ehrhardt, M., 1999. Methods of Seawater Analysis 3rd Edison Completely Revised and, Extended edition. Wiley- VCH. ISBN 3-527-29589-5.
Gurumurthy, G.P., Balakrishna, K., Riotte, J., Braun, J.J., Audry, S., Shankar, U.H.N., Manjunatha, B.R., 2012. Controls on intense silicate weathering in a tropical river, southwestern India. Chem. Geol. 300–301, 61–69.
Gurumurthy, G.P., Balakrishna, K., Tripti, M., Audry, S., Riotte, J., Braun, J.J., Udaya Shankar, H.N., 2014. Geochemical behaviour of dissolved trace elements in a monsoon-dominated tropical river basin, Southwestern India. Environ. Sci. Pollut. Res. 21, 5098–5120. https://doi.org/10.1007/s11356-013-2462-7.
Gurumurthy, G.P., Balakrishna, K., Tripti, M., Riotte, J., Audry, S., Braun, J.J., Lambs, L., Udaya Shankar, H.N., 2015a. Sources of major ions and processes affecting the geochemical and isotopic signatures of subsurface waters along a tropical river, Southwestern India. Environ. Earth Sci. 73, 333–346.
Gurumurthy, G.P., Balakrishna, K., Tripti, M., Riotte, J., Audry, S., Braun, J.J., Udaya Shankar, H.N., 2015b. Use of Sr isotopes as a tool to decipher the soil weathering processes in a tropical river catchment, southwestern India. Appl. Geochem. 63, 498–506.
Hughes, H.J., Sondag, F., Cocquyt, C., Laraque, A., Pandi, A., André, L., Cardinal, D., 2011. Effect of seasonal biogenic silica variations on dissolved silicon fluxes and isotopic signatures in the Congo River. Wiley Online Libr. 56, 551–561.
Hughes, H.J., Bouillon, S., André, L., Cardinal, D., 2012. The effects of weathering variability and anthropogenic pressures upon silicon cycling in an intertropical watershed (Tana River, Kenya). Chem. Geol. 308–309, 18–25.
Hughes, H.J., Sondag, F., Santos, R.V., André, L., Cardinal, D., 2013. The riverine silicon isotope composition of the Amazon Basin. Geochim. Cosmochim. Acta 121, 637–651.
Humborg, C., Blomqvist, S., Avsan, E., Bergensund, Y., Smedberg, E., Brink, J., Mörth, C.-M., 2002. Hydrological alterations with river damming in northern Sweden: Implications for weathering and river biogeochemistry. Glob. Biogeochem. Cycles 16, 12-1-12–13.
Integrated Hydrological Data Book, 2012. Central Water Commission. Delhi, New.
Karl, D.M., Tien, G., 1992. MAGIC: a sensitive and precise method for measuring dissolved phosphorus in aquatic environments. Limnol. Oceanogr. 37, 105–116. Available at: http://doi.wiley.com/10.4319/lo.1992.37.1.0105.
Lele, S., Srinivasan, V., Jamwal, P., Thomas, B.K., Eswar, M., Md. Zuhail, T., 2013. Water Management in Arkavathy Basin: A situational analysis. In: Environment and Development Discussion Paper.
Mangalaa, K.R., Cardinal, D., Brajard, J., Rao, D.B., Sarma, N.S., Djouraev, I., Chiranjeevulu, G., Murty, K.N., Sarma, V.V.S.S., 2017. Silicon cycle in Indian estuaries and its control by biogeochemical and anthropogenic processes. Cont. Shelf Res. 148, 64–88.
Meunier, J.D., Riotte, J., Braun, J.J., Sekhar, M., Chalié, F., Barboni, D., Saccone, L., 2015. Controls of DSi in streams and reservoirs along the Kaveri River, South India. Sci. Total Environ. 502, 103–113.
Mukherjee, A., Saha, D., Harvey, C.F., Taylor, R.G., Ahmed, K.M., Bhanja, S.N., 2015. Groundwater systems of the Indian Sub-Continent. J. Hydrol. 4, 1–14. https://doi.org/10.1016/J.EJRH.2015.03.005.
Naqvi, S.M., Rogers, J.W., 1987. Precambrian Geology of India. Clarendon Press, Oxford University Press, New York.
Opfergelt, S., Delmelle, P., 2012. Silicon isotopes and continental weathering processes: Assessing controls on Si transfer to the ocean. Compt. Rendus Geosci. 344, 723–738.
Pacheco, F., van der Weijden, C.H., 1996. Contributions of Water-Rock Interactions to the Composition of Groundwater in Areas with a Sizeable Anthropogenic Input: a Case Study of the Waters of the Fundão Area, Central Portugal. Water Resour. Res. 32, 3553–3570. https://doi.org/10.1029/96WR01683.
Pattanaik, J.K., Balakrishnan, S., Bhutani, R., Singh, P., 2007. Chemical and strontium isotopic composition of Kaveri, Palar and Ponnaiyar rivers: Significance to weathering of granulites and granitic gneisses of southern Peninsular India. Curr. Sci. 93 (4), 523–531.
Pattanaik, J.K., Balakrishnan, S., Bhutani, R., Singh, P., 2013. Estimation of weathering rates and CO2 drawdown based on solute load: significance of granulites and gneisses dominated weathering in the Kaveri River basin, Southern India. Geochim. Cosmochim. Acta 121, 611–636.
Poitrasson, F., 2017. Silicon isotope geochemistry. Rev. Mineral. Geochem. 82, 289–344.
Reynolds, B.C., Aggarwal, J., André, L., Baxter, D., Beucher, C., Brzezinski, M.A., Engström, E., Georg, R.B., Land, M., Leng, M.J., Opfergelt, S., Rodushkin, I., Sloane, H.J., van den Boorn, S.H.J.M., Vroon, P.Z., Cardinal, D., 2007. An inter-laboratory comparison of Si isotope reference materials. J. Anal. At. Spectrom. 22, 561–568. Available at: https://pubs.rsc.org/en/content/articlehtml/2007/ja/b616755a.
Reynolds, B.C., Georg, R.B., Oberli, F., Wiechert, U., Halliday, A.N., 2006. Re-assessment of silicon isotope reference materials using high-resolution multi-collector ICP-MS. J. Anal. At. Spectrom. 21, 266–269. https://doi.org/10.1039/B515908C.
Riotte, J., Meunier, J.D., Zambardi, T., Audry, S., Barboni, D., Anupama, K., Prasad, S., Chmeleff, J., Poitrasson, F., Sekhar, M., Braun, J.J., 2018a. Processes controlling silicon isotopic fractionation in a forested tropical watershed: Mule Hole critical Zone Observatory (Southern India). Geochim. Cosmochim. Acta 228, 301–319.
Riotte, J., Sandhya, K., Prakash, N.B., Audry, S., Zambardi, T., Chmeleff, J., Buvaneshwari, S., Meunier, J.D., 2018b. Origin of silica in rice plants and contribution of diatom Earth fertilization: insights from isotopic Si mass balance in a paddy field. Plant Soil 423, 481–501.
Sarma, V.V.S.S., Gupta, S.N.M., Babu, P.V.R., Acharya, T., Harikrishnachari, N., Vishnuvardhan, K., Rao, N.S., Reddy, N.P.C., Sarma, V.V., Sadhuram, Y., Murty, T.V.R., Kumar, M.D., 2009. Influence of river discharge on plankton metabolic rates in the tropical monsoon driven Godavari estuary, India. Estuar. Coast. Shelf Sci. 85, 515–524.
Savage, P.S., Georg, R.B., Williams, H.M., Turner, S., Halliday, A.N., Chappell, B.W., 2012. The silicon isotope composition of granites. Geochim. Cosmochim. Acta 92, 184–202.
Savage, P.S., Georg, R.B., Williams, H.M., Halliday, A.N., 2013. The silicon isotope composition of the upper continental crust. Geochim. Cosmochim. Acta 109, 384–399.
Schaller, J., Puppe, D., Kaczorek, D., Ellerbrock, R., Sommer, M., 2021. Silicon cycling in soils revisited. Plants 10, 295. Available at: https://www.mdpi.com/2223-7747/10/2/295.
Shadakshara Swamy, N., Jayananda, M., Janardhan, A.S., 1995. Geochemistry of Gundlupet gneisses, Southern Karnataka: A 2.5 Ga old reworked sialic crust. In: India as a Fragment of East Gondwana. Gondwana Research Group.
Struyf, E., Smis, A., Van Damme, S., Garnier, J., Govers, G., Van Wesemael, B., Conley, D.J., Batelaan, O., Frot, E., Clymans, W., Vandevenne, F., Lancelot, C., Goos, P., Meire, P., 2010. Historical land use change has lowered terrestrial silica mobilization. Nat. Commun. 1, 1–7.
Sutton, J.N., André, L., Cardinal, D., Conley, D.J., De Souza, G.F., Dean, J., Dodd, J., Ehlert, C., Ellwood, M.J., Frings, P.J., Grasse, P., Hendry, K., Leng, M.J., Michalopoulos, P., Panizzo, V.N., Swann, G.E.A., 2018. A review of the stable isotope bio-geochemistry of the global silicon cycle and its associated trace elements. Front. Earth Sci. 5, 112.
Tardy, Y., 1971. Characterization of the principal weathering types by the geochemistry of waters from some European and African crystalline massifs. Chem. Geol. 7, 253–271.
Thiry, M., 2000. Palaeoclimatic interpretation of clay minerals in marine deposits: an outlook from the continental origin. Earth Sci. Rev. 49, 201–221. https://doi.org/10.1016/S0012-8252(99)00054-9.
Tréguer, P.J., Sutton, J.N., Brzezinski, M., Charette, M.A., Devries, T., Dutkiewicz, S., Ehlert, C., Hawkings, J., Leynaert, A., Liu, S.M., Monferrer, N.L., López-Acosta, M., Maldonado, M., Rahman, S., Ran, L., Rouxel, O., 2021. Reviews and syntheses: the biogeochemical cycle of silicon in the modern ocean. Biogeosciences 18, 1269–1289. https://doi.org/10.5194/BG-18-1269-2021.
Vandevenne, F., Struyf, E., Clymans, W., Meire, P., 2012. Agricultural silica harvest: have humans created a new loop in the global silica cycle? Front. Ecol. Environ. 10, 243–248. Available at: http://doi.wiley.com/10.1890/110046.
Violette, A., Goddéris, Y., Maréchal, J.C., Riotte, J., Oliva, P., Kumar, M.S.M., Sekhar, M., Braun, J.J., 2010. Modelling the chemical weathering fluxes at the watershed scale in the Tropics (Mule Hole, South India): Relative contribution of the smectite/kaolinite assemblage versus primary minerals. Chem. Geol. 277, 42–60. https://doi.org/10.1016/J.CHEMGEO.2010.07.009.
WRIS, 2014. Kaveri Basin Report: Gov. of India - MoWR, 141.
Zabowski, D., Ugolini, F.C., 1992. Seasonality in the mineral stability of a subalpine Spodosol. Soil Sci. 154 (6), 497–507.